crystals

MDPI

Article

Effect of Rare Earth Yttrium on Inclusion Characteristics of Grain-Oriented Silicon Steel

Zhihong Guo [1], Xiangyang Li [1], Yu Liu [1], Yaxu Zheng [1,*], Liguang Zhu [1,*], Yuanxiang Zhang [2], Huilan Sun [1], Jie Feng [1] and Ruifang Cao [3]

[1] Hebei Key Laboratory of Material Near-Net Forming Technology, School of Material Science and Engineering, Hebei University of Science and Technology, Shijiazhuang 050018, China; guozhihong191@163.com (Z.G.); jaylee_liyan@163.com (X.L.); lylyly4231@163.com (Y.L.); sunhuilan1949@163.com (H.S.); hbgyfj@163.com (J.F.)
[2] State Key Laboratory of Rolling Technology and Automation, School of Material Science and Engineering, Northeastern University, Shenyang 110003, China; zhangyuanxiang@ral.neu.edu.cn
[3] Rolling Operation Department, Beijing Shougang Co., Ltd., Tangshan 064404, China; caoruifang2160@sgqg.com
* Correspondence: zhengyaxu1984@163.com (Y.Z.); zhulg@ncst.edu.cn (L.Z.)

Abstract: To investigate the influence of heavy rare earth element yttrium on the type, morphology, and quantity distribution of inclusions in grain-oriented silicon steel, thermodynamic calculation was carried out on the typical rare earth inclusions in grain-oriented silicon steel containing yttrium. The main inclusions in the experimental steels with and without yttrium were observed and analyzed using field emission scanning electron microscope (FESEM, Zeiss Gemini SEM 300) and energy dispersive spectrometer (EDS, OXFORD Ultim Extreme). The electron backscatter diffraction (EBSD, OXFORD Symmetry) was used to analyze the local average misorientation of the hot-rolled plate. The results show that the inclusions in the Y-free steel are mainly long MnS, irregular Al_2O_3 and MnS-Al_2O_3. The inclusions in the Y-bearing steel are spherical rare earth compounds. The number of inclusions in Y-bearing steel decreases and the size increases compared with Y-free steel. The mean value of local average misorientation and the dislocation density of Y-bearing steel are smaller compared with Y-free steel, which could avoid the cracking problem caused by dislocation accumulation during hot rolling. After heating the rough-rolling sample to 1350 °C, there is no obvious difference in the inclusions type between the Y-free steel and Y-bearing steel. However, the area fraction of inclusions in Y bearing steel increases slightly. According to the thermodynamic calculation results, there are mainly three kinds of rare earth inclusions, YS, Y_2S_3 and Y_2O_2S, in Y-bearing steel, among which YS has the strongest stability and the stability of Y_2O_2S is the weakest. The rare earth element yttrium can effectively modify the inclusions, transforming the irregular Al_2O_3 inclusions, formed during the deoxidation of silicon steel into spherical rare earth inclusions, which suppress the precipitation of long MnS inclusions. Thus, the formability of the steel could be improved.

Keywords: rare earth yttrium; grain-oriented silicon steel; inclusion; thermodynamics

check for updates

Citation: Guo, Z.; Li, X.; Liu, Y.; Zheng, Y.; Zhu, L.; Zhang, Y.; Sun, H.; Feng, J.; Cao, R. Effect of Rare Earth Yttrium on Inclusion Characteristics of Grain-Oriented Silicon Steel. *Crystals* **2023**, *13*, 896. https://doi.org/10.3390/cryst13060896

Academic Editor: Maria Milanova

Received: 19 April 2023
Revised: 24 May 2023
Accepted: 28 May 2023
Published: 30 May 2023

Copyright: © 2023 by the authors. Licensee MDPI, Basel, Switzerland. This article is an open access article distributed under the terms and conditions of the Creative Commons Attribution (CC BY) license (https://creativecommons.org/licenses/by/4.0/).

1. Introduction

Grain-oriented silicon steel is an important soft magnetic alloy with Si content of 2.9~3.4%, which has excellent magnetic properties such as high magnetic induction, low iron loss, and low magnetostriction. At present, it is mainly used in power, electronics and military industries. It is also used to manufacture iron cores of transformers and large motor stators [1–3]. The prior research showed that the cleanliness of silicon steel has an important influence on its magnetic properties. However, with the current melting process, there must be a certain amount of non-metallic inclusions and other impurities in the finished steel. The number, size, and density distribution of inclusions affect the microstructure and formability of grain-oriented silicon steel [4,5]. Reducing the number

and size of inclusions and reasonably controlling the characteristics of inclusions in steel are important to improve the magnetic properties of silicon steel. In grain-oriented silicon steel, the inhibitor-forming element Al will form irregular Al_2O_3 inclusions in the deoxidation stage, and the Mn element will also form large-sized plastic MnS inclusions. Reasonable control of the quantity and density distribution of Al_2O_3 and MnS inclusions is the key factor to ensure the preparation of high-quality grain-oriented silicon steel.

China is rich in rare earth resources. At the same time, China is one of the countries with a complete industrial chain of rare earth. The electronic structure of rare earth atoms determines its chemical properties. Generally, there are three electrons in the outermost or secondary layer of rare earth elements that are most likely to be lost. Therefore, rare earth metals are very easy to react with oxygen, sulfur, and other elements to generate compounds with high melting points, thus achieving the role of purifying molten steel. Moreover, adding rare earth elements to silicon steel can modify inclusions and refine the primary recrystallization structure, improving the as-cast structure and properties [6–8]. Studies have shown that rare earth cerium and lanthanum can effectively reduce the number of non-metallic inclusions in grain-oriented silicon steel, change the morphology of inclusions, and make the hot-rolled plate structure and the inhibitor distribution more uniform [9–11]. Compared with the light rare earth elements cerium and lanthanum, the heavy rare earth element yttrium has a smaller atomic radius and better solid solution effect in molten steel. In addition, the rare earth yttrium element and its formed oxygen sulfides are distributed at grain boundaries, playing a role in pinning grain boundaries and inhibiting grain growth [12–14]. It is reported that the inclusions in the pipeline steel and ship plate steel are mainly spherical or ellipsoidal Y_2O_3, Y_2O_2S, Y_2S_3, and YS inclusions with the addition of yttrium-based rare earth. The Al_2O_3 inclusions in the steel are modified into rare earth compounds, and the mechanical properties of steel are improved [15–17]. Studying the influence of rare earth elements on the characteristics of inclusions in oriented silicon steel is an important basis for determining whether rare earth elements can be used as alloy elements. At present, there are few articles analyzing the effect of rare earth yttrium on the inclusion characteristics of oriented silicon steel. The effects of yttrium on the type, composition, size, and morphology of inclusions in grain-oriented silicon steel were studied in this paper, and the influence mechanism was illustrated by thermodynamic calculation. It is beneficial to accelerate the application of rare earth elements in oriented silicon steel and provide data reference for the development of high-grade oriented silicon steel.

2. Materials and Methods

The experimental steel was obtained by smelting and casting in a 50 kg vacuum induction furnace, and its basic material is Fe-3wt% silicon steel. The chemical composition is shown in Table 1; 1 # steel does not contain Y, and the Y content in 2 # steel is 0.078%. The addition method of rare earth yttrium is to put it into the bottom of the mold in advance and dissolve it evenly in the molten steel. The yield of Y is 36.5%. The ingot was heated to 1150 °C and kept for 0.5 h, and then rough rolled 6 times to a size of 1000 mm × 200 mm × 20 mm steel plate. The rough-rolled plate was then hot rolled with 5 passes to become a plate with a thickness of 2.5 mm. The normalizing temperature is 920 °C, and the holding time is 5 min; the test steel was taken out for air cooling to 900 °C, and then cooled to room temperature by water spraying. The rolling and heat treatment process is shown in Figure 1.

Table 1. Chemical composition of 3% Si-oriented silicon steel (mass fraction, %).

Number	C	Si	Mn	P	S	Als	N	O	Y
1#	0.050	2.98	0.22	0.01	0.018	0.028	0.0043	0.0021	—
2#	0.014	2.97	0.22	0.01	0.011	0.035	0.0045	0.0020	0.078

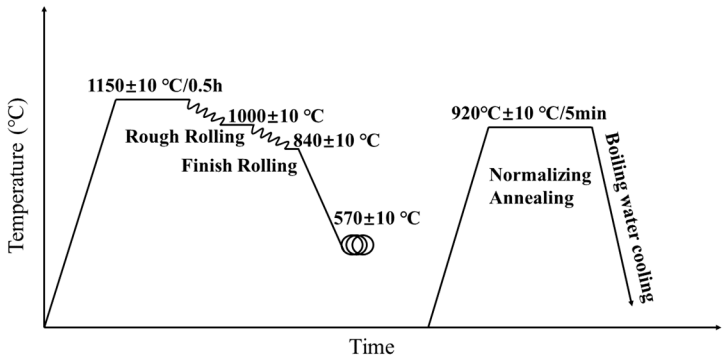


Figure 1. The schematic diagram of rolling and heat treatment process.

Samples with the size of 10 mm × 8 mm × 2.5 mm were taken from the experimental steels, which were used for inclusions detection and analysis. The samples were mechanically ground and polished, then slightly corroded with 4% nitric acid alcohol to eliminate surface stress, cleaned with deionized water and anhydrous ethanol, then dried by cold air. Field emission scanning electron microscopy (FESEM, Zeiss Gemini SEM 300, Oberkochen, Germany) and its attached energy spectrometer (EDS, OXFORD Ultim Extreme, Oxfordshire, UK) were used to analyze the number and density distribution and chemical composition of large-sized inclusions in the test steel. At the same time, typical inclusions were selected and their morphology and composition were determined [18,19].

Electron backscatter diffraction (EBSD, OXFORD Symmetry, Oxfordshire, UK) was used to analyze the local average orientation difference of hot-rolled plates. When observing texture, sample preparation is usually divided into conventional polishing and electrolytic polishing methods. When observing hot-rolled plates, electrolytic polishing is used, with an electrolyte of 5% perchloric acid, a voltage of 25–30 V, and an electrolytic time of 5-10 s. The EBSD scanning step of a hot-rolled plate is 2 μm. The scanning area is 3 mm, and the data obtained after scanning are analyzed using CHANNEL 5 software. The morphology and quantity of inclusions were observed and statistically analyzed using transmission electron microscopy (TEM, FEI Tecnai G2 F20 S-TWIN, Hillsboro, USA), and the composition of inclusions was qualitatively analyzed using energy dispersive spectroscopy (EDS, FEI Tecnai G2 F20S-TWIN, Hillsboro, USA). TEM samples were prepared by carbon coating method.

3. Results and Discussion

3.1. Effect of Rare Earth Y on the Type and Morphology of Inclusions in Hot-Rolled Plates and Normalized Plates

The statistical results of the type and quantity of inclusions in Y-bearing and Y-free hot-rolled and normalized plates are shown in Tables 2 and 3, where N represents the total number of inclusions per unit area, and the d_{mean} is the average size of inclusions in the corresponding silicon steel plate. The analysis shows that the inclusions in the test steel without rare earth Y are mainly MnS, Al_2O_3 single-phase inclusions, and Al_2O_3-MnS composite inclusions. With the progress of rough rolling, finishing rolling, and normalizing process, the total number of inclusions in the test steel increases gradually, but the type of inclusions remains the same. With the addition of rare earth Y, the amount of rare earth sulfur oxide inclusions in the test steel increases greatly, the Al_2O_3-MnS type inclusions are transformed into Y_xS_y-Y_2O_2S rare earth inclusions, and the single-phase MnS inclusion disappears. In addition, there are a small amount of large-sized Al_2O_3 inclusions.

Table 2. Type and quantity statistics of inclusions in Y-free silicon steel plate.

Steel Sample	Inclusion Type	N/pcs	d_{mean}/μm
Rough rolled plate	MnS, Al_2O_3-MnS	301	1.59
Finish rolled plate	MnS, Al_2O_3-MnS	388	1.36
Normalized plate	MnS, Al_2O_3-MnS	397	1.58

Table 3. Type and quantity statistics of inclusions in Y-bearing silicon steel plate.

Steel Sample	Inclusion Type	N/pcs	d_{mean}/μm
Rough rolled plate	Y_xS_y-Y_2O_2S, Al_2O_3	248	2.17
Finish rolled plate	Y_xS_y-Y_2O_2S, Al_2O_3	266	1.92
Normalized plate	Y_xS_y-Y_2O_2S, Al_2O_3	266	2.22

Figure 2 shows the composition and morphology of inclusions in rough-rolled plates without Y. Elliptical MnS inclusions and irregular Al_2O_3-MnS type inclusions are mainly found in the rough-rolled plates. Due to the high solid solution temperature of MnS, the size of MnS inclusions in the rough-rolling stage is relatively large, with most of the MnS sizes being around 2 μm. The solid solution temperature of Al_2O_3 is very high. Before the steel liquid solidifies, Al_2O_3 already exists. During the cooling process of the steel liquid, the particles that precipitate later are easy to precipitate and grow with the existing particles as the core. Therefore, a large part of the inclusions in the rough-rolled plate are composite inclusions with Al_2O_3 as the core; as the size of Al_2O_3 as the core itself is about 2 μm, the generated composite inclusions are larger in size, around 5 μm. Due to the small reduction in rough rolling, the deformation of inclusions is also less affected.

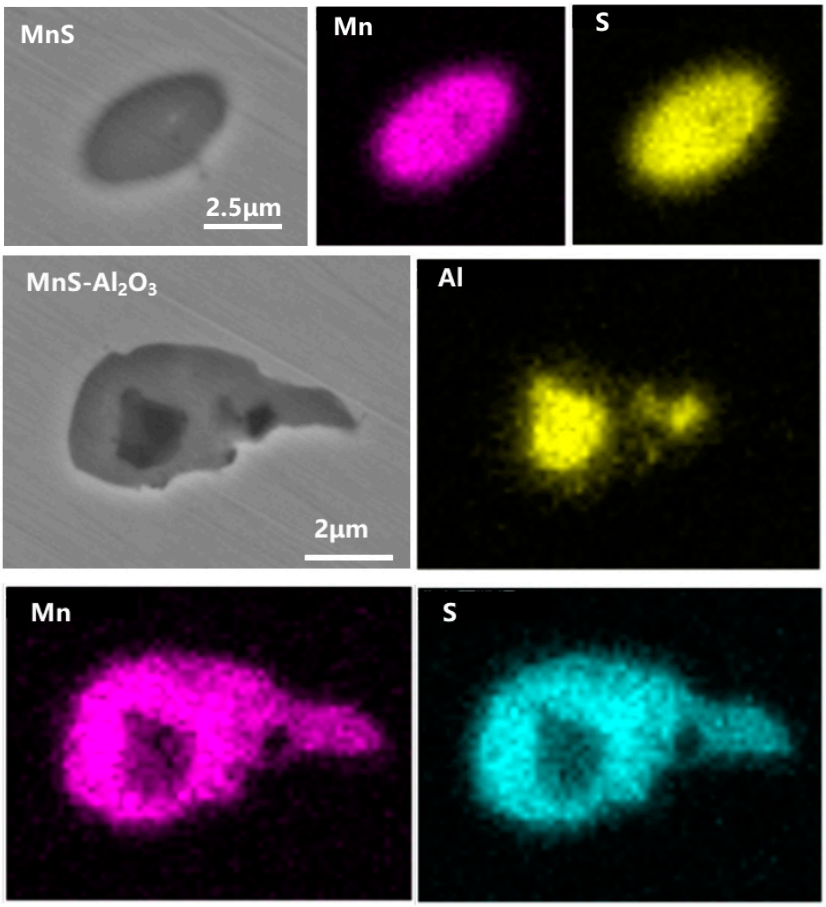


Figure 2. Composition and morphology of inclusions in the rough-rolled steel plate without Y.

Figure 3 shows the composition and morphology of inclusions in the Y-free precision rolled steel plate. Compared with the rough-rolled plate, the main types of inclusions have not changed, mainly consisting of MnS inclusions and Al_2O_3-MnS composite inclusions. Unlike rough-rolled plates, MnS inclusions change from elliptical to elongated shapes because MnS has high plasticity and extends with deformation under large deformation variables. The Al_2O_3-MnS composite inclusion is formed by Al_2O_3 as the core, which has the characteristic of high hardness. Under large reduction, the Al_2O_3-MnS composite inclusion does not deform and its size does not change.

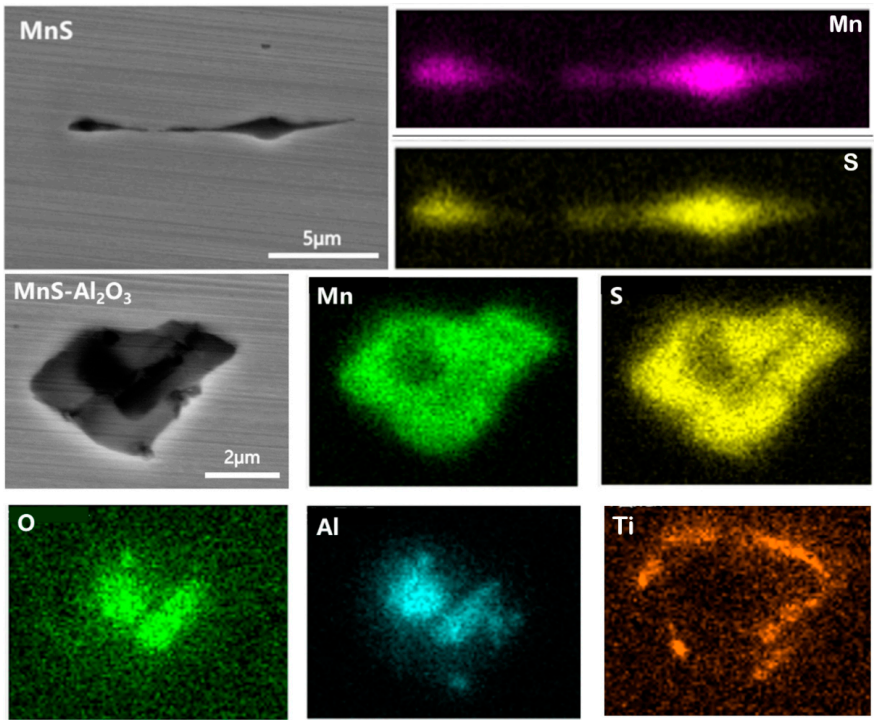


Figure 3. Composition and morphology of inclusions in finish-rolled steel plate without Y.

Figure 4 shows the composition and morphology of inclusions in a normalized plate without Y. The inclusions in the normalized plate after normalization treatment are mainly elliptical MnS and irregular Al_2O_3-MnS. Unlike rough and finish-rolled plates, MnS inclusions are finer, with a size of around 600 nm. This is because during normalization treatment, as the temperature increases, MnS solidly dissolves into the austenite phase, and as the temperature decreases, fine and dispersed MnS precipitates. However, there are still some large-sized Al_2O_3-MnS composite inclusions remaining in the normalization plate, which is because the lower normalization temperature did not completely dissolve MnS.

With the addition of rare earth Y, the composition and morphology of inclusions in the steel are shown in Figure 5. The inclusions in rough-rolled plate, finish-rolled plate and normalizing plate are all transformed into spherical or ellipsoidal Y_xS_y-Y_2O_2S type inclusions. There are no MnS or MnS-Al_2O_3 type inclusions in Y-bearing silicon steel. Rare earth Y is easy to combine with oxygen and sulfur in molten steel to form spherical yttrium sulfide, yttrium sulfur oxide or other type inclusions containing yttrium, which can effectively inhibit the formation of long strip MnS inclusions in the steel. Due to the strong deoxidization ability of rare earth, most of the Al_2O_3 inclusions in steel are also modified into rare earth sulfur oxides. Spherical or ellipsoidal rare earth sulfides are dispersed in the steel matrix and maintain their original morphology during rolling [20–24]. The residual Al_2O_3 inclusions have a larger size and a strip-shaped morphology, with a relatively small quantity, which will not affect the mechanical properties of the steel.

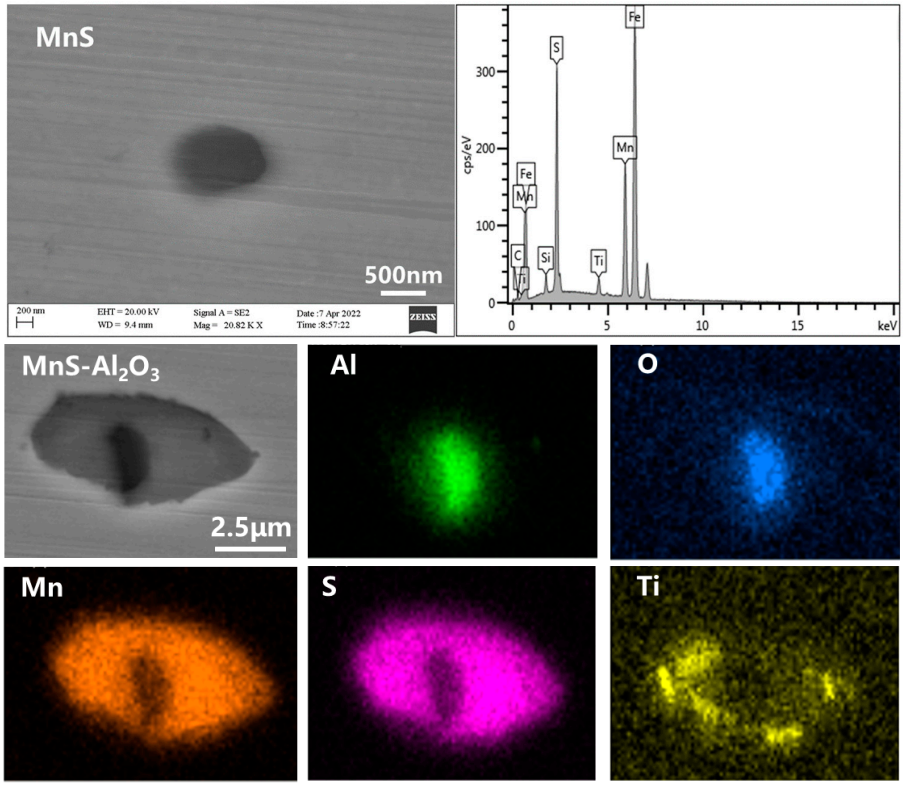


Figure 4. Composition and morphology of inclusions in the normalized steel plate without Y.

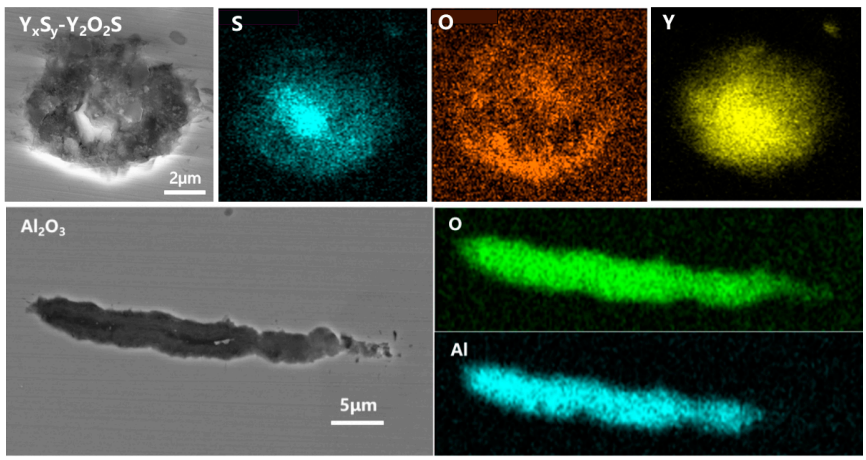


Figure 5. Composition and morphology of inclusions in Y-bearing steel.

The morphology and composition of micro inclusions in the hot-rolled plate of the test steel were observed by TEM and EDS. The results are shown in Figures 6 and 7. Spherical MnS-SiO_2 composite precipitates with a size less than 200 nm are mainly found in Y-free steel. From the element distribution diagram, it can be seen that the distribution of S element is relatively high, and MnS precipitates with SiO_2 as the core composite. In the Y-bearing steel, there are spherical particles with a size of about 20 nm, which are distributed in an aggregated state. The EDS analysis results show that the particles are mainly composed of O, Si, S, Mn, and Y. No Al containing particles and single fine MnS precipitation were found in the experimental steel [25]. From the distribution maps of various elements, it can be seen that small inclusions adhere to the SiO_2 matrix, with a relatively low content of Mn element. The aggregated small particles are mostly rare earth oxide sulfides.

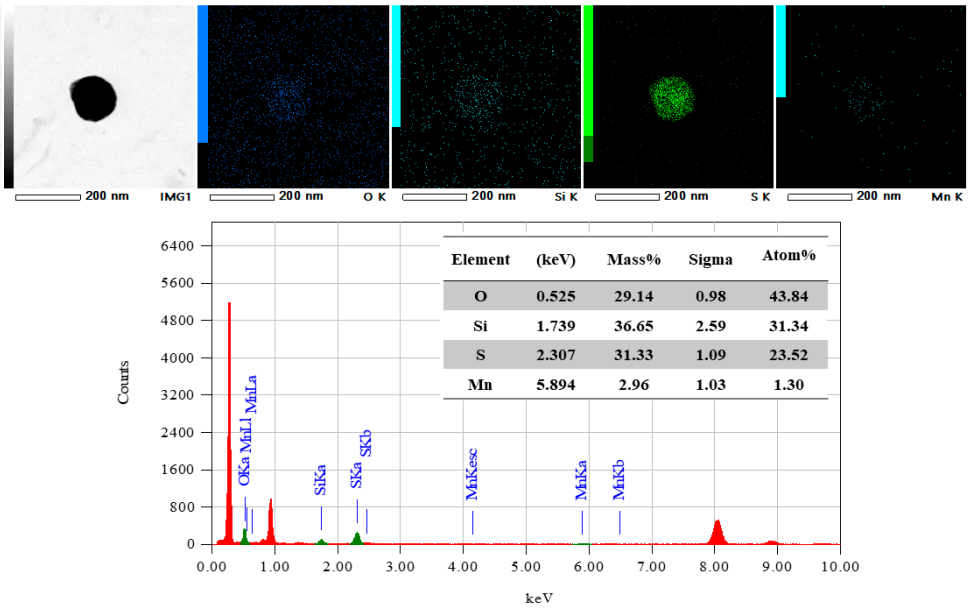


Figure 6. Composition distribution of fine precipitates in Y-free steel.

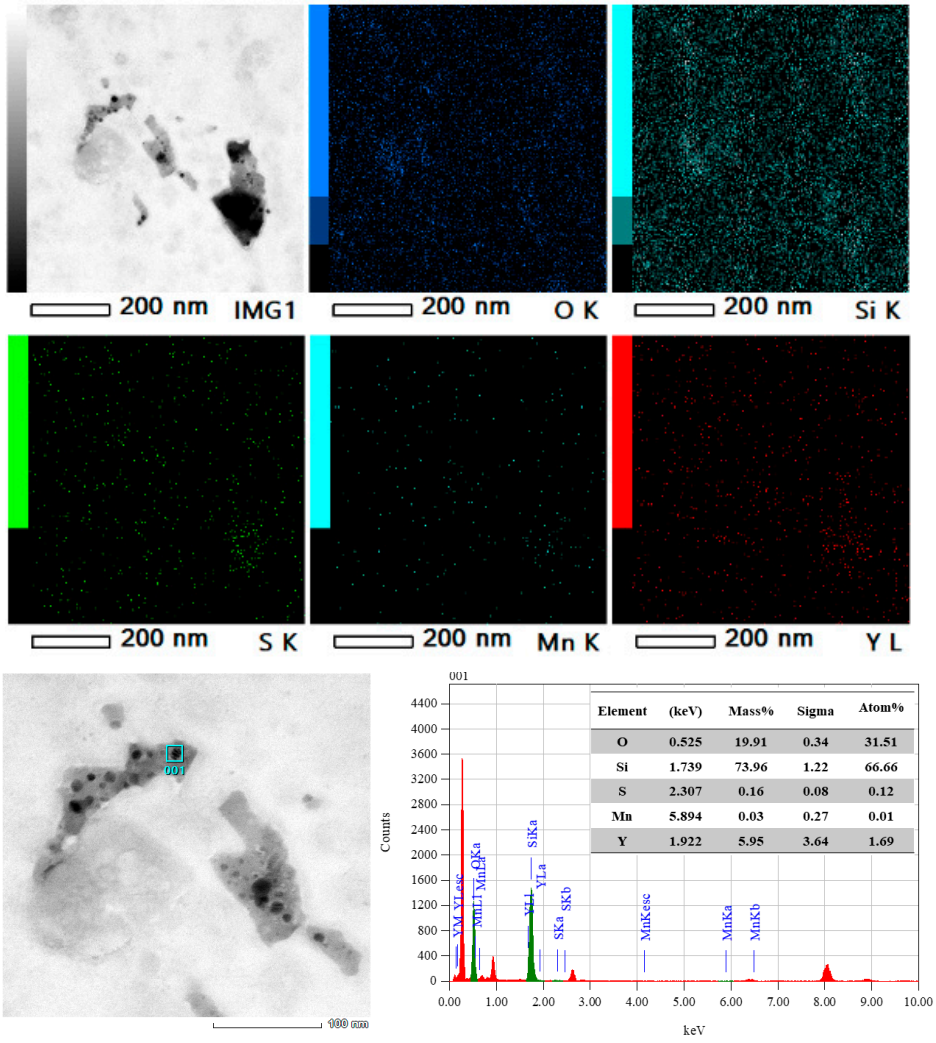


Figure 7. Composition distribution of fine precipitates in Y-bearing steel.

3.2. Effect of Rare Earth Y on Inclusions Composition in the Hot-Rolled Plate and Normalized Plate

Inclusion data in 30 consecutive fields of view were collected using a field emission scanning electron microscope (FE-SEM) with a magnification of 500 times. The density of inclusions is expressed by N, as shown in Formula (1), that is, the number of inclusions within a certain size range detected in the unit field of view area of the sample, unit: pieces/mm^2. Among them, the N_t represents the total number of inclusions in all fields of view, unit: pieces, and A_t represents the total area of all fields of view, unit: mm^2. The inclusion area fraction is expressed by the percentage of the inclusion area to the total field of view area in a certain size range detected in the steel, % [11,26].

$$N = \frac{N_t}{A_t} \tag{1}$$

The quantity density and area fraction of inclusions in different size ranges in the rough-rolled plates are shown in Figure 8. With the addition of rare earth Y, the number of inclusions in the rough-rolled plate decreased as a whole, in which the inclusions in the size range of 0.5~2 μm decreased by 29%. However, the number of larger size inclusions increased significantly, and the inclusions in the size range of 2~4 μm increased by about 1.5 times. Compared with the samples without rare earth Y, the area fraction of inclusions in Y-bearing steel increases generally. The area fraction of inclusions smaller than 4 μm is 0.171%, and the area fraction of inclusions larger than 4 μm is 0.086%.

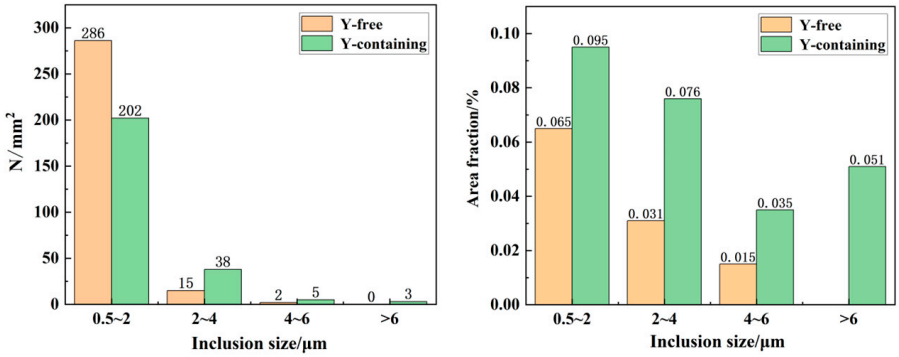


Figure 8. Quantity density and area fraction of inclusions in the rough-rolled plate.

The quantity density and area fraction of inclusions in different size ranges in the finish-rolled plate are shown in Figure 9. With the addition of rare earth Y, the number of inclusions in the finish-rolled plate is greatly reduced, in which the number of inclusions within the size range of 0.5~2 μm is reduced by 48%, and the number of inclusions within the size range of 2~4 μm is increased by 14%. The area fraction of inclusions smaller than 4 μm in finish-rolled steel plates containing yttrium decreased to some extent. However, there are many inclusions with a size larger than 4 μm in the Y-bearing finish-rolled plate. The area fraction of inclusions in the Y-bearing finish-rolled plate increased obviously. Compared with the samples without rare earth, the area fraction of inclusions in Y-bearing steel is obviously higher.

The quantity density and area fraction of inclusions in different size ranges in the normalized plate are shown in Figure 10. With the addition of rare earth Y, the number of inclusions in the normalized plate is still reduced overall, among which the number of small size inclusions in the range of 0.5~2 μm is reduced by 38%, and the inclusions in the range of 2~4 μm are reduced by 11%. Similar to the hot-rolled plate, there are still many inclusions larger than 4 μm in the Y-containing normalizing plate. These large-sized inclusions lead to a significant increase in the area fraction of inclusions in normalized plates containing yttrium. Compared with the samples without rare earth, the area fraction of inclusions with the size of 0.5~2 μm reduces by 0.069%, with the size of 2~4 μm increases by 0.017%, with the size of 4~6 μm increases by 0.064%, and that of the inclusions larger

than 6 μm increases by 0.048%. The addition of rare earth yttrium reduces the area fraction of small-sized inclusions and increases the area fraction of large-sized inclusions.

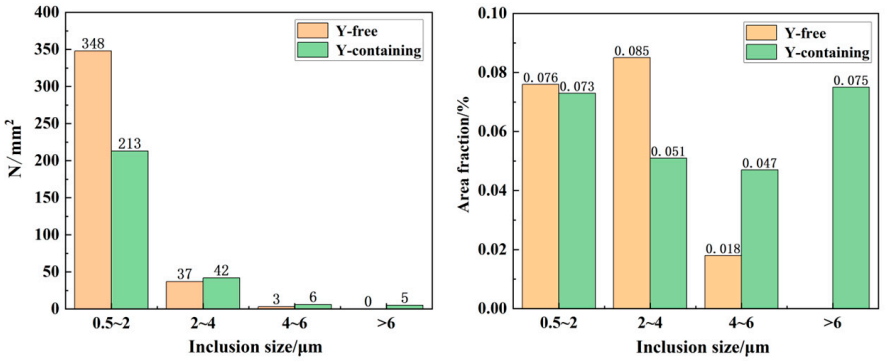


Figure 9. Quantity density and area fraction of inclusions in finish-rolled plate.

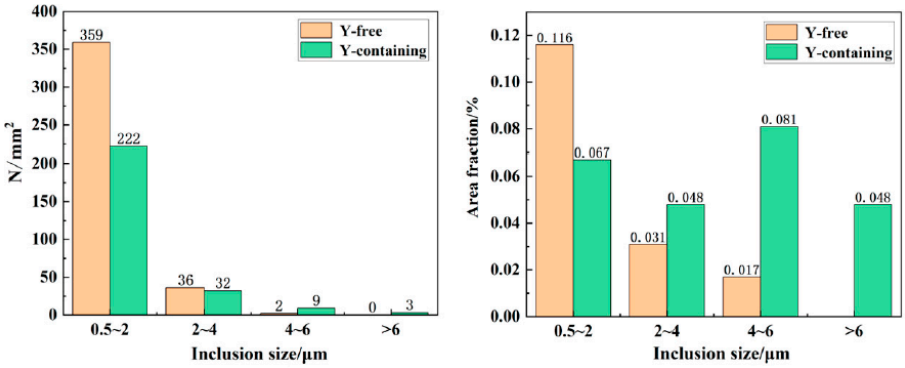


Figure 10. Quantity density and area fraction of inclusions in the normalized plate.

The addition of rare earth yttrium inhibits the nucleation of small-sized inclusions such as MnS and Al_2O_3, and reduces the number and area fraction of small-sized inclusions in the steel. At the same time, large-sized rare earth containing inclusions are formed in the steel. With rough rolling, finishing rolling, and normalization progress, the number of small-sized inclusions in Y-free steel increases significantly. This is due to the uniform and fine precipitation of MnS during the rolling process, and the number of large-sized inclusions has no obvious change. According to the statistical results of inclusions area fraction, the area fraction of small-sized inclusions in Y-free steel increases obviously with the progress of the rolling and annealing processes. The number of inclusions in Y-bearing steel increases slightly in the three processes, and the area fraction of small-sized inclusions decreases, while that of large-sized inclusions increases. The author believes that this is due to the heating treatment of different processes, which increases the size of rare earth inclusions within a certain size range. In general, due to the relatively large amount of rare earth in the experimental steel, the number of inclusions larger than 4 μm increases, but the average size of the inclusions only increases about 0.60 μm.

3.3. Morphological Characteristics of Inclusions in Test Steel after Solid Solution Heat Treatment

Samples with the size of 10 mm × 8 mm × 8 mm were taken from two kinds of test steels. Put the sample into a 1350 °C tube furnace, keep it for 20 min, and then put it into cold water to cool to room temperature. The morphology of inclusions is shown in Figures 11 and 12. The inclusions in Y-free steel are mainly irregular Al_2O_3 and strip or spherical MnS-Al_2O_3 inclusions, and no MnS inclusions are detected. This is because the solution temperature of MnS in the steel is about 1320 °C, and the sample is heated to 1350 °C and kept for 20min in the experiment, which made MnS a solid solution again. The inclusions in the Y-bearing steel are still spherical YxSy-Y_2O_2S inclusions, and the high-temperature heating does not affect the inclusion types of the Y-bearing steel.

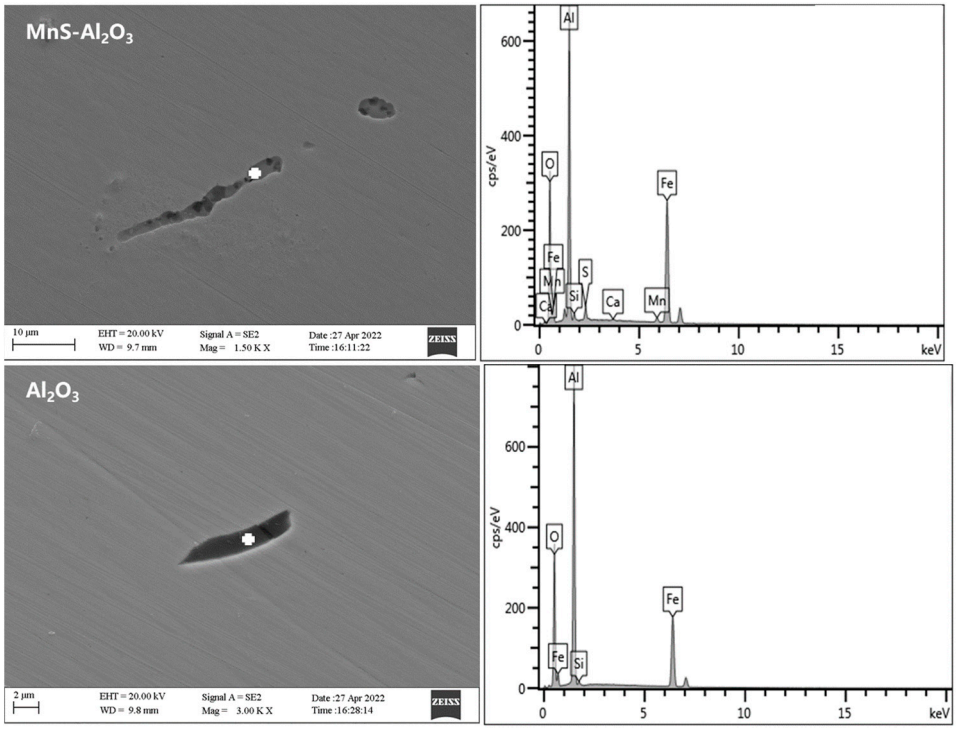


Figure 11. Composition and morphology of inclusions in Y-free steel after high-temperature heating.

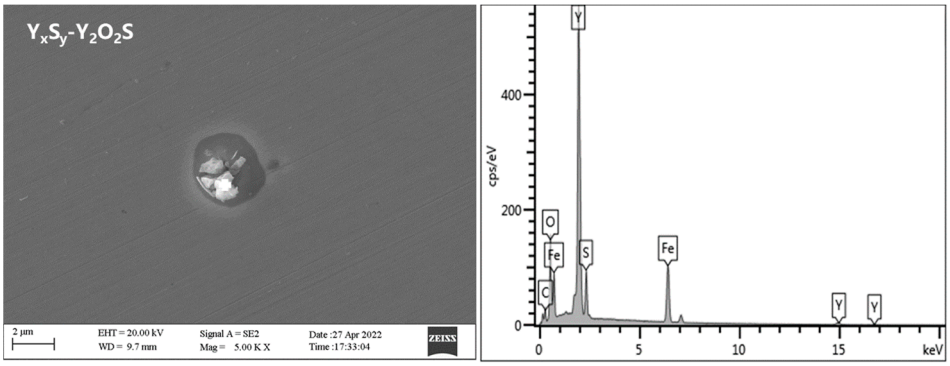


Figure 12. Composition and morphology of inclusions in Y-bearing steel after high-temperature heating.

The quantity density and area fraction of inclusions in the rough-rolled plate heated at high temperature are shown in Figure 13. Compared with Y-bearing steel and Y-free steel, the number of small inclusions in the size range of 0.5~2 μm in the Y-free steel is reduced by 41%, and inclusions in the size range of 2~4 μm are reduced by 62%. However, there are still many large-sized inclusions in the Y-bearing steel, which are larger than 4 μm. The inclusions area fraction of Y-free steel is also significantly lower than that of Y-bearing steel. According to Figures 6 and 11, since most MnS inclusions in the steel are redissolved at high temperatures, the number and area fraction of inclusions in the Y-free steel are significantly reduced. However, the area fraction of inclusions in Y-bearing steel increases slightly, which is consistent with the results of the above experiments. The high heating temperature before hot rolling makes the MnS and other inhibitors in the grain-oriented silicon steel dissolve again, and fine particles are precipitated during hot rolling. With the addition of rare earth yttrium, the inclusions in steel are transformed into high melting point rare earth inclusions due to the denaturation effect of rare earth on inclusions. With the high heating temperature at 1350 °C, only the area fraction of inclusions in Y-bearing steel increased slightly.

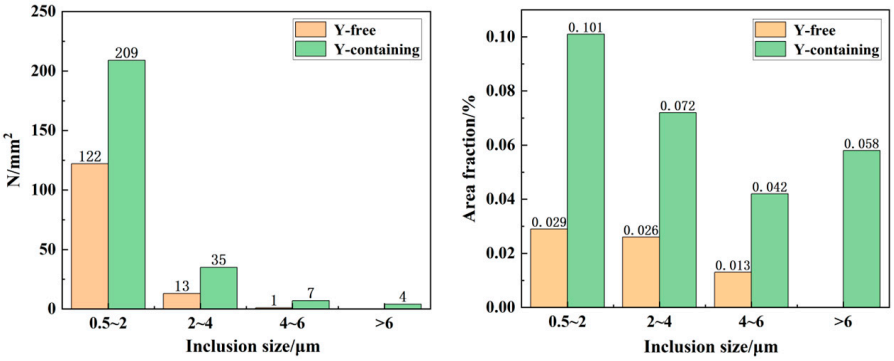


Figure 13. Quantity density and area fraction of inclusions in experimental steel with high heating temperature.

3.4. Influence of Rare Earth Y on the Formability of Hot-Rolled Plate

Figure 14a,b represent the local average orientation difference (LAM) of hot-rolled plates, Y-free and Y-bearing, respectively. By scanning the orientation difference between adjacent data points in the grain using EBSD, and statistical analysis of LAM, the orientation change inside the grain of plastic deformed metal after deformation is analyzed. The small angle orientation difference between grains can form substructure grain boundaries and dislocations, so although dislocation density cannot be directly measured, the relative size of dislocation density can be measured through statistical LAM [27]. The dislocation density increases with the increase of the deformation variable, so the LAM value is indirectly positively correlated with the dislocation density, that is, the higher the overall dislocation density, the greater the LAM value.

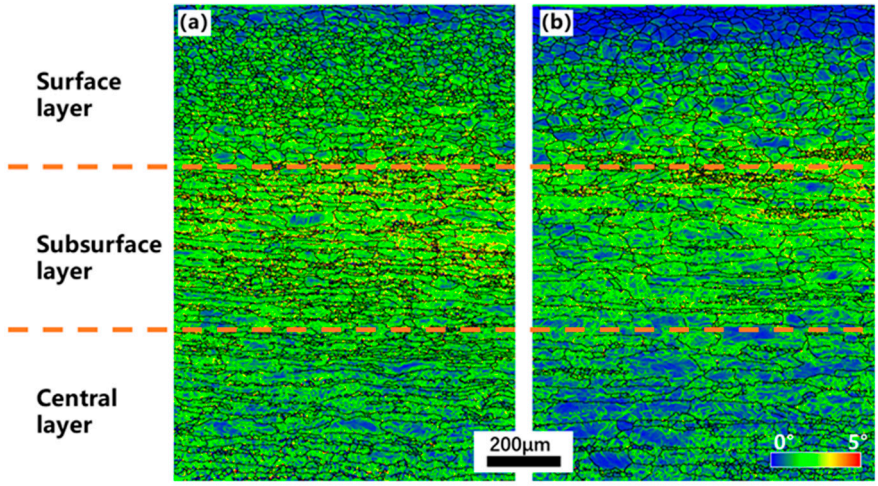


Figure 14. Distribution diagram of LAM of hot-rolled sheet: (**a**) Y-free; (**b**) Y-bearing.

The LAM values are shown in Figure 15, where the abscissa represents the LAM value and the ordinate represents the relative frequency. The peak values of LAM of hot-rolled plates without and containing Y appeared at 1.05° and 0.75°, respectively, and the average values of local orientation difference were 1.72° and 1.40°, respectively. This shows that the number of data points with higher local misorientation decreases after adding rare earth. There are strip MnS inclusions and irregular Al_2O_3 inclusions in the traditional hot-rolled plate of grain-oriented silicon steel. Due to the presence of these inclusions, when the interface deformation is incompatible with the matrix, dislocation accumulation is easy to occur at the interface, which makes the stress and strain distribution more uneven [28]. Stress concentration areas are easily formed at the interface. In addition, there is an area between the inclusion and the steel matrix where the stress gradient is not obvious. If the inclusion is close enough, that is, the number density of the inclusion is relatively high,

the stress fields around the inclusion may interact and cause stress concentration [29,30]. With the addition of rare earth, the inclusions such as MnS and Al_2O_3 in the hot-rolled plate are transformed into spherical rare earth compounds, and the number of small- and medium-sized inclusions in steel is significantly reduced. This improves the mechanical properties of the hot-rolled silicon steel plate and avoids the cracking problem caused by dislocation accumulation during the hot-rolling process.

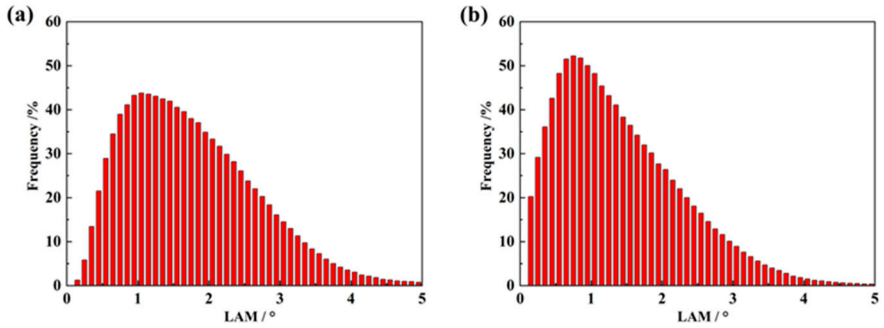


Figure 15. LAM statistical chart of hot-rolled plate: (**a**) Y-free; (**b**) Y-bearing.

4. Thermodynamic Calculation Results and Analysis

4.1. Thermodynamic Analysis of Rare Earth Inclusions

Due to the low electronegativity of rare earth elements, they have a strong ability for deoxidation and desulfurization. The addition of rare earth elements in steel will form rare earth compounds containing sulfur and oxygen. Four inclusions of Y_2O_3, Y_2O_2S, Y_2S_3, and YS may be formed after the addition of rare earth in grain-oriented silicon steel [31–33]. To analyze the formation and change of rare earth inclusions in the test steel, the thermodynamic calculation is used to analyze and discuss them. The formation reaction formulas and standard Gibbs free energies of formation of four rare earth compounds at 1600 °C are shown in Table 4.

Table 4. Formation reaction formulas and standard Gibbs free energies of formation of rare earth compounds.

Chemical Reaction Formula	ΔG^{θ}/(J·mol^{-1})
2[Y] + 3[O] = Y_2O_3(s)	−1792600 + 658.0T
2[Y] + 2[O] + [S] = Y_2O_2S(s)	−1521000 + 536.0T
2[Y] + 3[S] = Y_2S_3(s)	−1171000 + 441.0T
[Y] + [S] = YS(s)	−321080 + 91.0T

According to Equations (2)–(6), the Gibbs free energy of the reaction can be obtained [34].The reaction of any rare earth element in steel can be expressed by the following general formula:

$$[RE] + \frac{M}{N}[F] = \frac{1}{N}RE_NF_M \quad (2)$$

$[RE]$ is the rare earth element, $[F]$ is the reactant, RE_NF_M is the product, N and M are the number of atoms of rare earth elements and reactants in the product. Gibbs free energy of formation can be obtained from the isothermal equation:

$$\Delta G = \Delta G^{\theta} + RTlnJ \quad (3)$$

Among them, ΔG^{θ} is the standard Gibbs free energy of formation, unit: J/mol; R is the gas constant, which is generally taken as 8.314 J/(mol·k); T is the thermodynamic temperature, unit: K; J is the activity product, and its calculation formula is:

$$J = \frac{\left(a_{RE_NF_M}\right)^{\frac{1}{N}}}{a_{RE}\left(a_F\right)^{\frac{M}{N}}} \quad (4)$$

Since the mass fraction of each solute in the molten steel tends to 0 and the mass fraction of the solvent tends to 1, the mass fraction of 1% is selected as the standard state. The activity a_i of any component i in steel is expressed by the following formula:

$$a_i = f_i \omega[i] \tag{5}$$

where f_i is the activity coefficient. The calculation method is the Wagner model. Under isothermal and equal pressure, for Fe-2-3- system, it is considered that the logarithm of the activity coefficient f_2 of component 2 of the multiple system is a function of the concentration of each component [2%], [3%], and the simplified calculation formula of the model is as follows:

$$lgf_i = \sum_{j=1}^{n} e_i^j \omega[j] \tag{6}$$

In the formula, e_i^j is the activity interaction coefficient of element j to solute i. $\omega[i]$ and $\omega[j]$ are the mass percentage of i, j in molten steel, respectively. The activity interaction coefficient of relevant elements in molten steel at 1600 °C is shown in Table 5 [35,36].

Table 5. Interaction coefficient of elements in molten steel at 1600 °C.

e_i^j	C	Si	Mn	P	S	O	N	Al	Y
O	−0.450	−0.131	−0.021	0.070	−0.133	−0.20	0.057	−3.900	−16.300
S	0.112	0.063	−0.026	0.029	−0.028	−0.27	0.01	0.035	−0.550
Y	−0.220	—	—	—	−7.340	−90.70	−0.875	—	−0.006
Al	0.091	0.0056	0.035	0.033	0.030	−6.60	−0.058	0.045	—

Henry activity coefficients and Henry activities of O, S, Y and Al in molten steel are calculated according to the above Wagner model. The results are shown in Table 6. The activities of the four rare earth compounds Y_2O_3, Y_2O_2S, Y_2S_3, and YS in the molten steel at 1600 °C are 1. According to Formulas (3) and (4), the Gibbs free energy of the formation of rare earth compounds is obtained, and the results are shown in Table 7.

Table 6. Activity coefficient and activity of various elements of Y-bearing steel at 1600 °C.

$f_{[O]}$	$a_{[O]}$	$f_{[S]}$	$a_{[S]}$	$f_{[Y]}$	$a_{[Y]}$	$f_{[Al]}$	$a_{[Al]}$
0.01553	0.00003	1.38283	0.01521	0.53749	0.04192	1.03367	0.04651

Table 7. Gibbs free energy of each reaction formula of Y-bearing steel at 1600 °C.

Chemical Reaction Formula	*J*	Δ*G*, J/mol
$2[Y] + 3[O] = Y_2O_3(s)$	1.89×10^{17}	23,456.912
$2[Y] + 2[O] + [S] = Y_2O_2S(s)$	3.87×10^{13}	−29,879.46
$2[Y] + 3[S] = Y_2S_3(s)$	1.62×10^{8}	−50,675.21
$[Y] + [S] = YS(s)$	1.57×10^{3}	−36,062.01

According to the physical meaning of Gibbs free energy, when $\Delta G < 0$, the reaction proceeds forward; when $\Delta G > 0$, the reaction proceeds backward. It can be found from the calculation results of Table 7, $\Delta G(Y_2O_3)$ = 23,456.92 J/mol, and that Y_2O_3 inclusions cannot be precipitated in molten steel Y-bearing at 1600 °C. $\Delta G(Y_2O_2S)$ = −29,879.46 J/mol, $\Delta G(Y_2S_3)$ = −50,675.21 J/mol, ΔG(YS) = −36,062.01 J/mol, the Gibbs free energy of formation of Y_2O_2S, Y_2S_3, and YS is less than 0, so these three kinds of inclusions can be precipitated from the Y-bearing steel.

4.2. Mutual Conversion of Rare Earth Inclusions

The rare earth inclusions precipitated from molten steel cannot exist stably all the time, which is related to the actual production environment and the mutual transformation of inclusions. The reaction formula for the experiment's mutual transformation of the three rare earth inclusions is shown in Table 4.

$$[Y] + YS(s) + 2[O] = Y_2O_2S(s)\ \Delta G^{\theta} = -1{,}199{,}920 + 445T \quad (7)$$

$$2YS(s) + [S] = Y_2S_3(s)\ \Delta G^{\theta} = -528{,}840 + 259T \quad (8)$$

$$Y_2S_3(s) + 2[O] = Y_2O_2S(s) + 2[S]\ \Delta G^{\theta} = -350{,}000 + 95T \quad (9)$$

Formula (7) is the conversion reaction between YS and Y_2O_2S. Combined with the above relevant data and formulas, it is concluded that the Gibbs free energy of formation of the reaction is 6182.56 J/mol; it can be known that the reaction is carried out in reverse, the Y_2O_2S inclusions precipitated in the molten steel will be transformed into YS inclusions, that is, the stability of YS is better. According to the conversion reaction formula between YS and Y_2S_3 in Formula (8), it is calculated that the Gibbs free energy of formation of the reaction is 19448.82 J/mol, and the reaction proceeds in the reverse direction. The reaction formula between Y_2S_3 and Y_2O_2S is shown in Formula (9). After calculation, the Gibbs free energy of formation of the reaction is 20,795.75 J/mol, and the reaction proceeds in reverse. It can be seen that when the Y content is 0.078%, the stability of the three rare earth inclusions in the molten steel at 1600 °C is YS>Y_2S_3>Y_2O_2S, that is, YS will preferentially precipitate. However, due to the limitation of the reaction balance, the conversion reaction between rare earth inclusions will not proceed completely, so YS, Y_2S_3, and Y_2O_2S will exist in the molten steel at the same time.

4.3. Evolution of Al_2O_3 Inclusions in Y-Bearing Grain-Oriented Silicon Steel

In the smelting process of grain-oriented silicon steel without yttrium, Al will be added to the molten steel for deoxidation, so Al_2O_3 inclusions will inevitably be generated in the steel. The morphology of Al_2O_3 is generally irregular, and its thermal expansion coefficient is significantly different from that of the steel matrix, therefore, it is easy to cause cracks in the steel during the rolling process. The thermal expansion coefficient of rare earth inclusions are similar to that of steel substrates, avoiding the generation of cracks at the interface between rare earth inclusions and steel substrates during steel processing, thereby improving the impact resistance of the steel. With the addition of rare earth yttrium, since the affinity of Y to O and S is stronger than that of Al, rare earth yttrium has a metamorphic effect on Al_2O_3 inclusions [37]. The formation reaction formula and standard Gibbs free energy of the formation of Al_2O_3 are as follows:

$$2[Al] + 3[O] = Al_2O_3(s)\ \Delta G^{\theta} = -1{,}205{,}198 + 387.72T \quad (10)$$

The conversion reaction formula between Al_2O_3 and Y_2O_2S is:

$$6[Y] + 2Al_2O_3(s) + 3[S] = 3Y_2O_2S(s) + 4[Al]\ \Delta G^{\theta} = -2{,}152{,}764 + 832.56T \quad (11)$$

From the calculation results, it is known that the Gibbs free energy of formation of the above formula is −292,574.63 J/mol, and the reaction is going forward, that is, with the addition of rare earth Y in molten steel, Y can transform Al_2O_3 into Y_2O_2S. However, it is still limited by the reaction equilibrium, and a small amount of Al_2O_3 remains in the steel. According to the influence of rare earth yttrium on the modification effect of inclusion, the diagram of inclusion modification is drawn as shown in Figure 16. To sum up, the inclusions in the steel containing yttrium are mainly yttrium sulfide, yttrium sulfur oxide, and its composite inclusions. In addition, there are residual Al_2O_3 inclusions, which are consistent with the test results.

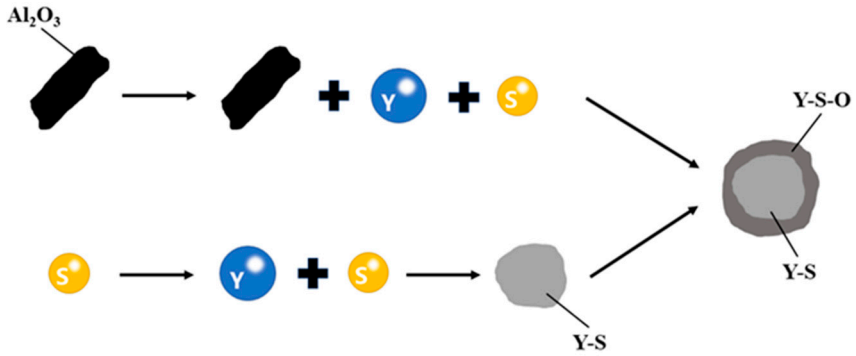


Figure 16. Schematic diagram of inclusion modification after adding rare earth yttrium.

5. Conclusions

(1) In the Y-free silicon steel, the inclusions are mainly strip MnS, irregular Al_2O_3, and MnS-Al_2O_3. With the addition of rare earth Y, the inclusions in the test steel changed into spherical rare earth compounds, and the average size of the inclusions increased significantly. The addition of rare earth Y effectively improves the morphology of inclusions, especially the large-sized MnS and Al_2O_3 inclusions. The spheroidizing modification of inclusions in steel is obvious, which is beneficial for improving the plasticity of steel.

(2) In roughing and finishing hot-rolling and normalizing processes, the number and area fraction of smaller inclusions in Y-free steel gradually increase. There is no obvious change in the number of inclusions in the roughing, finishing, and normalizing samples of Y-bearing steel, but the area fraction of inclusions increases slightly. The addition of rare earth reduces the precipitation amount of irregular large-sized inclusions in the steel. Due to the relatively large addition of rare earth in the experimental steel, the number of inclusions with a size of more than 4 μm increased, but the average size of inclusions increases by only about 0.60 μm. When the rough-rolling sample is heated at 1350°C, the characteristics of rare earth inclusions in Y-bearing steel are relatively stable, and only the area fraction increases slightly.

(3) Through thermodynamic calculation, when the yttrium content is 0.078%, three kinds of rare earth inclusions, YS, Y_2S_3, and Y_2O_2S, mainly existed in the steel. The stability of YS is the strongest, and that of Y_2O_2S is the weakest. The addition of rare earth yttrium can denature the Al_2O_3 inclusions formed by deoxidation of the silicon steel, and inhibit the precipitation of long strips of MnS. Reasonable controlling of liquid steel composition and rare earth addition can effectively control the characteristics of inclusions in the steel.

Author Contributions: Conceptualization, Y.Z. (Yaxu Zheng) and L.Z.; Data curation, X.L.; Formal analysis, Z.G.; Funding acquisition, Z.G.; Investigation, X.L., Y.Z. (Yuanxiang Zhang), H.S., J.F., Y.L. and R.C.; Methodology, Y.Z. (Yaxu Zheng); Project administration, Z.G.; Resources, X.L. and Y.Z. (Yuanxiang Zhang); Software, X.L.; Supervision, Y.Z. (Yaxu Zheng) and L.Z.; Validation, Z.G. and X.L.; Visualization, R.C.; Writing-original draft, X.L.; Writing-review and editing, Y.Z. (Yaxu Zheng) and Z.G. All authors have read and agreed to the published version of the manuscript.

Funding: This research was funded by the National Nature Science Foundation of China under grant numbers 51974102, 52204341, 51974103, 52204342, and 52174311, Hebei Provincial Foundation under grant numbers E2021208006, E2021208017, and E2019208308, and Key R & D projects in Hebei Province grant numbers QN2019029, 20311003D, and 19211009D.

Institutional Review Board Statement: Not applicable.

Informed Consent Statement: Not applicable.

Data Availability Statement: Not applicable.

Conflicts of Interest: The authors declare no conflict of interest.

References

1. Etter, A.L.; Baudin, T.; Penelle, R. Influence of the Goss grain environment during secondary recrystallization of conventional grain-oriented Fe-3%Si steels. *Scr. Mater.* **2002**, *47*, 725–730. [CrossRef]
2. Hayakawa, Y.; Kurosawa, M. Orientation relationship between primary and secondary recrystallized texture in electrical steel. *Acta Mater.* **2002**, *50*, 4527–4534. [CrossRef]
3. Wang, L.; Wang, S.; Li, J.; Liang, J.; Feng, Y. Effect of Slab Reheating Temperature on Cold Rolling Texture Evolution of Nb-Containing Grain-Oriented Silicon Steel. *Crystals* **2021**, *11*, 1478.
4. Jenkins, K.; Lindenmo, M. Precipitates in electrical steels. *J. Magn. Magn. Mater.* **2008**, *320*, 2423–2429.
5. Garza Montes de Oca, N.F.; Pineda Arriaga, K.Y.; Gaona Martínez, M.J.; Ramírez Ramírez, J.H.; Pérez González, F.A.; Colás, R. Surface and Subsurface Defects Formed in a Cold-Rolled Electrical Steel. *J. Fail. Anal. Prev.* **2023**, *23*, 298–305. [CrossRef]
6. He, Z.; Sha, Y.; Gao, Y.; Chang, S.; Zhang, F.; Zuo, L. Recrystallization texture development in rare-earth (RE)-doped non-oriented silicon steel. *J. Iron Steel Res. Int.* **2020**, *27*, 1339–1346. [CrossRef]
7. Li, H.; Li, M.; Liu, D.; Li, A.; Ma, Y. Effects of yttrium on microstructure, elevated-temperature tensile properties and fracture mechanism of 6.5% Si non-oriented electrical steel. *Electr. Steel* **2022**, *4*, 18–24.
8. Wu, Z.; Jin, Z.; Ren, H.; Liu, R.; Li, T.; Zhang, X. Investigation on the primary and secondary recrystallization textures of rare earth micro-alloyed grain-oriented silicon steel. *J. Phys. Conf. Ser.* **2019**, *1270*, 012003. [CrossRef]
9. Qu, M.; Ren, H.; Jin, Z.; Yang, J.; Li, Y. Effect of Ce on microstructure and inhibitor evolution for 3% grain-oriented steel. *Heat Treat. Met.* **2017**, *42*, 26–30.
10. Zhang, X.; Jin, Z.; Ren, H.; Wu, Z. Effect of rare earth Ce on as-cast precipitates of Cu-containing low-temperature grain-oriented silicon steel. *Heat Treat. Met.* **2020**, *45*, 135–139.
11. Xie, X.; Liu, Y.; Li, G.; Chen, X.; Zhu, C. Effect of Ce-La alloying treatment on characteristics of inclusions in grain-oriented silicon steels. *Iron Steel* **2021**, *56*, 122–134.
12. Darling, K.A.; VanLeeuwen, B.K.; Koch, C.C.; Scattergood, R.O. Thermal stability of nanocrystalline Fe–Zr alloys. *Mater. Sci. Eng. A* **2010**, *527*, 3572–3580. [CrossRef]
13. Bugnet, M.; Kula, A.; Niewczas, M.; Botton, G.A. Segregation and clustering of solutes at grain boundaries in Mg–rare earth solid solutions. *Acta Mater.* **2014**, *79*, 66–73. [CrossRef]
14. Park, H.K.; Han, C.H.; Park, C.S.; Park, J.T.; Joo, H.D. Abnormal grain growth induced by grain boundary segregation of yttrium in grain-oriented Fe-3% Si steel. *Mater. Charact.* **2018**, *146*, 204–208. [CrossRef]
15. Yang, Q.; Yang, J.; Ding, H.; Liu, X. Thermodynamic analysis and observation of inclusions in RE-pipeline steel. *Chin. Rare Earths* **2018**, *39*, 96–101.
16. Zhao, M.; Wang, F.; Xi, X.; Yang, S.; Li, J. Effect of Y on inclusions characteristics and tensile properties in EH36 shipbuilding steek. *Iron Steel* **2019**, *54*, 61–67.
17. Luo, D.; Liu, M.; Jiang, X.; Yu, Y.; Zhang, Z.; Feng, X.; Lai, C. Effect of yttrium-based rare earth on inclusions and cryogenic temperature impact properties of offshore engineering steel. *Crystals* **2022**, *12*, 305. [CrossRef]
18. Zheng, Y.; Wang, Q.; Zhu, L.; Han, B.; Guo, Z.; Wang, B.; Feng, J.; Lu, S.; Shen, W.; Cao, R. Microstructure evolution and carbide precipitation behavior of microalloyed TS800TB steel during hot rolling and coiling processes. *Mater. Sci. Eng. A* **2022**, *840*, 142902. [CrossRef]
19. Zheng, Y.; Shen, W.; Zhu, L.; Guo, Z.; Wang, Q.; Feng, J.; Li, Y.; Cao, R.; Wu, J. Effects of composition and strain rate on hot ductility of Cr–Mo-alloy steel in the two-phase region. *High Temp. Mater. Process.* **2021**, *40*, 228–240. [CrossRef]
20. Torkamani, H.; Raygan, S.; Garcia Mateo, C.; Rassizadehghani, J.; Vivas, J.; Palizdar, Y.; San-Martin, D. The influence of La and Ce addition on inclusion modification in cast niobium microalloyed steels. *Metals* **2017**, *7*, 377. [CrossRef]
21. Kazuo, K.; Shiro, W.; Tokio, S. Phase Analysis of Sulfides of Rare Earth Elements in Steel. *Trans. Iron Steel Inst. Jpn.* **2019**, *18*, 212–220.
22. Torkamani, H.; Raygan, S.; Garcia Mateo, C.; Rassizadehghani, J.; Palizdar, Y.; San-Martin, D. Contributions of rare earth element (La, Ce) addition to the impact toughness of low carbon cast niobium microalloyed steels. *Met. Mater. Int.* **2018**, *24*, 773–788. [CrossRef]
23. Luo, D.; Yu, Y.; Zhang, Z.; Sun, L.; Feng, X.; Lai, C. Development of high impact toughness offshore engineering steel by yttrium-based rare earth addition. *Ironmak. Steelmak.* **2021**, *48*, 1247–1253.

24. Li, B.; Zhu, H.; Zhao, J.; Song, M.; Li, J.; Xue, Z. Effect of rare-earth La on inclusion evolution in high-Al Steel. *Steel Res. Int.* **2022**, *93*, 2100347. [CrossRef]
25. Zhu, L.; Li, X.; Zheng, Y.; Guo, Z.; Zhang, Y.; Sun, H.; Liu, P.; Liu, Y.; Cao, R. Effect of rare earth Y on microstructure and texture of oriented silicon steel during hot rolling and cold rolling processes. *High Temp. Mater. Process.* **2022**, *41*, 621–634.
26. Xiao, Y.; Liu, Y.; Huang, L.; Li, G.; Yan, W.; Zhu, C. Effect of acid-soluble aluminum and niobium content on inclusion characteristics of grain-oriented silicon steel. *J. Iron Steel Res.* **2022**, *34*, 543–554.
27. Meng, Y.; Ren, Q.; Ju, X. Evaluation of dislocation density by local grain misorientation in deformed metals. *Trans. Mater. Heat Treat.* **2014**, *35*, 122–128.
28. Du, Z.; Liu, X.; Gui, J.; Ke, Y.; Zhang, L. Influence of MnS inclusions on dynamic recrystallization and annealing twins formation during thermal deformation. *J. Mater. Res. Technol.* **2022**, *16*, 1371–1387. [CrossRef]
29. Arreola-Herrera, R.; Cruz-Ramírez, A.; Rivera-Salinas, J.E.; Romero-Serrano, J.A.; Sánchez-Alvarado, R.G. The effect of non-metallic inclusions on the mechanical properties of 32 CDV 13 steel and their mechanical stress analysis by numerical simulation. *Theor. Appl. Fract. Mech.* **2018**, *94*, 134–146. [CrossRef]
30. Guo, S.; Zhu, H.; Han, Y.; Li, J.; Xue, Z. State of the art for influence of inclusion on ductility and toughness of steel. *J. Iron Steel Res.* **2022**, *34*, 713–726.
31. Adabavazeh, Z.; Hwang, W.S.; Su, Y.H. Effect of adding cerium on microstructure and morphology of Ce-based inclusions formed in low-carbon steel. *Sci. Rep.* **2017**, *7*, 46503. [CrossRef]
32. Gerasin, S.; Kalisz, D.; Żak, P.L.; Kuglin, K.; Iwanciw, J. The effect of yttrium addition on the chemical composition of the non-metallic phase in liquid steel. *IOP Conf. Ser. Mater. Sci. Eng.* **2018**, *461*, 012093. [CrossRef]
33. Gerasin, S.; Kalisz, D.; Iwanciw, J. Thermodynamic characteristics of Y_2O_3 and Y_2S_3 nonmetallic phase formed in liquid steel. *Key Eng. Mater.* **2020**, *844*, 9–23. [CrossRef]
34. Chen, X.; Yang, S.; Li, J. Modification of Yttrium Containing E36 Shipboard Steel Inclusions. *J. China Metall.* **2019**, *29*, 25–30.
35. Wang, L.; Du, T. Thermodynamics of deoxidation, desulfuration and deoxysulfuration of yttrium in liquid iron. *Iron Steel* **1985**, *20*, 9–15.
36. Du, T. Thermodynamics of rare earth elements in iron-base solutions. *J. Iron Steel Res.* **1994**, *6*, 6–12.
37. Kalisz, D.; Żak, P.L.; Semiryagin, S.; Gerasin, S. Evolution of Chemical Composition and Modeling of Growth Nonmetallic Inclusions in Steel Containing Yttrium. *Materials* **2021**, *14*, 7113. [CrossRef]

Disclaimer/Publisher's Note: The statements, opinions and data contained in all publications are solely those of the individual author(s) and contributor(s) and not of MDPI and/or the editor(s). MDPI and/or the editor(s) disclaim responsibility for any injury to people or property resulting from any ideas, methods, instructions or products referred to in the content.